Quenching of the magnetic moment of Cr in $R\mathrm{Cr_2Si_2}$ compounds upon filling with carbon

V. Klosek,* A. Vernière, and B. Malaman
Laboratoire de Chimie du Solide Minéral, UMR 7555, Université Henri Poincaré, B.P. 239, 54506 Vandoeuvre-lès-Nancy Cedex, France

J. Tobola and S. Kaprzyk
Faculty of Physics and Applied Computer Science, AGH University of Science and Technology, Al. Mickiewicza 30, 30-059 Krakow, Poland

(Received 9 November 2007; revised manuscript received 1 July 2008; published 22 September 2008; corrected 2 October 2008)

Structural and magnetic properties of the $R\mathrm{Cr_2Si_2C}$ compounds (R=Y, La–Sm, Gd–Er) with the carbon-filled $\mathrm{CeMg_2Si_2}$-type structure (space group $P4/mmm$) have been studied by means of powder and single-crystal x-ray diffractions, magnetic measurements, and neutron powder diffraction. The compounds with R=Pr, Nd, Gd–Dy order ferromagnetically at low temperature ($T_C \leq 35$ K), whereas those with R=Y, La, Ce, and Sm do not exhibit any magnetic ordering down to 2 K. On the contrary, the "parent" $\mathrm{ThCr_2Si_2}$-type (space group $I4/mmm$) $R\mathrm{Cr_2Si_2}$ compounds (R=Y, Sm, Tb–Lu) exhibit strong antiferromagnetic properties ($T_N > 600$ K) linked to a large magnetic moment ($\sim 1.9\ \mu_B$) on the Cr sublattice. In order to better understand the role played by carbon on structural and magnetic properties in these systems, *ab initio* electronic structure calculations of $R\mathrm{Cr_2Si_2}$ and $R\mathrm{Cr_2Si_2C}$ compounds with R=Y and La have been performed, using the Korringa-Kohn-Rostoker (KKR) method, in the $\mathrm{ThCr_2Si_2}$- and $\mathrm{CeMg_2Si_2}$-types as well as their corresponding C-"filled" types, with C atoms located in Cr (001) planes. This study has allowed elucidating the particular role of carbon in the breakdown of the local magnetic moment on the Cr sublattice. KKR calculations clearly evidence that strong hybridization between d states on Cr atoms and p states on C atoms leads to a marked decrease in the density of states in the vicinity of E_F (well below the Stoner limit). Since similar electronic structure modifications are observed whatever the crystal structure, we tentatively conclude that the Cr-C interactions are more predominant in the disappearance of magnetism in $R\mathrm{Cr_2Si_2C}$ than the effect of the rearrangement of Si and R atomic planes when passing from the $\mathrm{ThCr_2Si_2}$ type to the $\mathrm{CeMg_2Si_2}$-type structure. Moreover, KKR calculations with the coherent-potential approximation undertaken for the "model" $R\mathrm{Cr_2Si_2C_x}$ system ($0 \leq x \leq 1$) well illustrate the evolution of the electronic structure and magnetic properties upon increasing carbon concentration.

DOI: 10.1103/PhysRevB.78.104419 PACS number(s): 61.50.−f, 61.66.Fn, 71.20.Be, 71.23.−k

I. INTRODUCTION

$R\mathrm{Cr_2Si_2}$ compounds, where R=Y, Sm, Tb–Lu, crystallize in the tetragonal $\mathrm{ThCr_2Si_2}$-type structure (space group $I4/mmm$), i.e., the ordered derivative of the binary $\mathrm{BaAl_4}$-type structure. Remarkably, these materials exhibit strong antiferromagnetic properties ($T_N \geq 600$ K) due to a large magnetic moment on the Cr sublattice ($\sim 1.96\ \mu_B$),[1–4] whereas the rare-earth sublattice orders antiferromagnetically at very low temperature ($T < 5$ K). The origin of the magnetic behavior in these Cr-containing RT_2X_2 compounds remains a subtle subject for band theory analysis, since, for example, the iron sublattice never orders magnetically in the isotype $R\mathrm{Fe_2}X_2$ silicides and germanides.[1,5] Moreover, it was earlier believed that magnetic moments on the transition-metal sublattice may appear in RT_2X_2 compounds only when T=Mn.[6]

A magnetic ground state of $\mathrm{YCr_2Si_2}$ was theoretically predicted by means of nonspin-polarized electronic structure calculations and applying the Stoner criterion.[4] The value of the Cr magnetic moment experimentally deduced from neutron-diffraction measurements has been supported by electronic structure investigations, using the Korringa-Kohn-Rostoker (KKR) method, accounting for the experimentally observed magnetic structure.[1,7]

Recently, new quaternary $R\mathrm{Cr_2Si_2C}$ silicides have been synthesized.[8–10] We reported on crystallographic studies showing that insertion of carbon stabilizes $R\mathrm{Cr_2Si_2C}$ compounds with a "filled" $\mathrm{CeMg_2Si_2}$-type structure (space group $P4/mmm$). This structure differs from the $\mathrm{ThCr_2Si_2}$ type only by the R and Si plane stacking along the c axis; C atoms being located within the Cr (001) planes.[9,10] This structural modification leads to lowering of point symmetry of atomic positions and a tetragonal body-centered structure is replaced with a primitive tetragonal one (with a two times smaller lattice constant c).

The goal of this paper is to experimentally and theoretically investigate the structural and magnetic properties of C inserted $R\mathrm{Cr_2Si_2C}$ compounds (R=Y, La–Sm, Gd-Er) by means of x-ray and neutron-diffraction experiments and magnetic susceptibility measurements as well as by applying the KKR method for electronic structure calculations (R=Y and La) especially to investigate magnetic behavior of the chromium sublattice.

II. EXPERIMENTAL PROCEDURES

Polycrystalline $R\mathrm{Cr_2Si_2C}$ samples (R=Y, La–Sm, Gd–Er) were prepared by direct combination of commercially available high-purity elements (yttrium and lanthanide ingots >99.9%; chromium ingots >99.9%; silicon >99.99%; carbon >99.9%). Using a high-frequency induction furnace under purified Ar atmosphere, stoichiometric amounts of the starting elements were melted in a water-cooled crucible.

TABLE I. Summary of data collection and structure refinement conditions for $LaCr_2Si_2C$, $SmCr_2Si_2C$, and YCr_2Si_2C.

	$LaCr_2Si_2C$	$SmCr_2Si_2C$	YCr_2Si_2C
Molar Mass (g mol^{-1})	311.10	322.54	261.10
Crystal dimensions (μm)	70*40*15	60*30*10	70*40*15
Symmetry	Tetragonal	Tetragonal	Tetragonal
a (Å)	4.048(1)	3.985(1)	3.969(2)
c (Å)	5.381(1)	5.279(2)	5.219(4)
V (Å^3)	88.17(6)	83.83(7)	82.21(15)
Z	1	1	1
ρ (g cm^{-3})	4.46	5.59	6.31
Space group	$P4/mmm$	$P4/mmm$	$P4/mmm$
Radiation	Mo Kα	Mo Kα	Mo Kα
Monochromator	Graphite	Graphite	Graphite
Scan mode	Oscillation	Oscillation	Oscillation
θ range	5°–35°	5°–27°	1°–31°
Linear abs. coeff. μ (mm^{-1})	18.4	24.1	24.0
Number of intensities:			
-recorded	372	160	239
-unique and nonzero	146	77	99
-kept [$I>2\sigma(I)$]	139	76	97
F (000)	139	144	121
Number of parameters	12	12	12
Final R value (%)	2.58	2.86	4.17
S (Goodness of fit)	0.977	1.205	1.197

Samples were remelted several times to ensure homogeneity. The purity of the resulting samples was checked with the powder x-ray diffraction technique (Guinier Co $K_{\alpha 1}$), high-purity silicon being used as an internal standard.

Single crystals of YCr_2Si_2C, $LaCr_2Si_2C$, and $SmCr_2Si_2C$ were extracted from the as-cast ingots and were mounted on a Nonius Kappa-CCD area detector x-ray diffractometer (Mo K_α, $\lambda=0.710\,73$ Å) at the Service Commun de Diffractométrie de l'Université de Nancy I. The conditions of data collection (DENZO software[11]) and structure refinements are gathered in Table I. The cell parameters were determined from reflections taken from one set of ten frames (1.0° steps in ϕ), each at 10 s exposure. The refinements were conducted using the SHELX97 software,[12] and the corrections for absorption were made using the SORTAV program.[13]

Macroscopic magnetic measurements were carried out on powders between 4.2 and 300 K on a DSM8 MANICS magnetosusceptometer in applied fields up to 1.5 T. The polycrystalline sample was fastened to the end of a rigid rod and then submitted to a horizontal force due to a magnetic-field gradient perpendicular to the rod axis. An applied torque then allowed bringing the rod back to its equilibrium position, and the intensity of the corresponding current needed to apply this torque was directly proportional to the magnetic susceptibility of the sample.

Powder neutron-diffraction experiments were performed at the Institut Laue Langevin (ILL, Grenoble, France). The diffraction patterns were recorded with the one-dimensional curved multidetector of the high-flux D1B diffractometer [$\lambda=2.524$ Å (Ref. 14)] in the temperature range 2–300 K and analyzed by the Rietveld method using the FULLPROF software.[15] In the case of $DyCr_2Si_2C$, a special double-walled vanadium sample holder was used to minimize absorption.

III. THEORETICAL DETAILS

Electronic structure calculations have been performed on RCr_2Si_2C (R=Y and La) employing crystallographic parameters deduced from our neutron-diffraction refinements (at $T=2$ K). We used the full-potential KKR method, whose formalism has been widely discussed by many authors,[16] with technical details shown in Ref. 17. In our computations we implemented the novel quasilinear algorithm[18] which allows for more precise and less time consuming band-structure calculations compared to conventional techniques. The full form of crystal potential was used (with no shape restriction to the spherical part only) over the whole atomic Voronoï cells, with l truncation on each atom up to $l_{max}=3$. Within the local-density approximation (LDA) approximation, the Perdew-Wang formula[19] for the exchange-correlation part of the crystal potential was applied. For finally converged atomic charges ($\sim 10^{-3}e$) and potentials (~ 1 mRy), the total, site-decomposed, and l-decomposed density of states (DOSs) were computed using the integration tetrahedron method in reciprocal space (120 k points in the irreducible part of the Brillouin zone). The Fermi level (E_F) was precisely determined from the Lloyd formula,[20] which appears to be particularly important in systems close to magnetic instability. In all figures presented here, E_F is located at zero, and nonspin-polarized DOS curves are given in Ry^{-1} per spin direction.

Spin-polarized KKR calculations have also been performed for RCr_2Si_2C compounds. They confirmed a nonmagnetic ground state, predicted earlier from the spin nonpolarized DOS and the Stoner product analysis. To gain better insight into the origin of magnetic ordering disappearance upon inserting carbon into the RCr_2Si_2 (R=Y and La) antiferromagnets, KKR calculations incorporating the coherent-potential approximation[21] (CPA) have also been carried out. In hypothetical $YCr_2Si_2C_x$, for $x=0.05$, 0.25, 0.5, 0.75, and 0.90, the nonspin-polarized DOS curves are illustrated and the behavior discussed in both structural models (the "filled" $ThCr_2Si_2$-type structure, space group $I4/mmm$ and the "filled" $CeMg_2Si_2$-type, space group $P4/mmm$). Moreover, spin-polarized KKR-CPA computations of $YCr_2Si_2C_x$ performed in the antiferromagnetic (AF) state allowed determining the Cr magnetic-moment variation versus C content.

In computations of existing structures, we have applied the experimental values of lattice constants and atomic positions, whereas in the case of hypothetical structures, the crystallographic parameters have been extrapolated from the aforementioned data. In particular, all lattice constants were linearly varied (i.e., $a=b$ expanded $\sim 2.3\%$, while c shrunk $\sim 1.1\%$ for $0<x<1$) when modeling the evolution of electronic structure and Cr magnetic moment in $YCr_2Si_2C_x$.

TABLE II. Lattice parameters of RCr_2Si_2C (R=La-Nd, Sm, Gd–Er, Y) compounds.

	a (Å)	c (Å)	V (Å^3)	c/a
$LaCr_2Si_2C$	4.048(1)	5.381(1)	88.2(1)	1.3293
$CeCr_2Si_2C$	4.012(2)	5.278(3)	85.0(1)	1.3156
$PrCr_2Si_2C$	4.0228(6)	5.351(2)	86.6(1)	1.3302
$NdCr_2Si_2C$	4.006(1)	5.320(1)	85.2(2)	1.3280
$SmCr_2Si_2C$	3.985(1)	5.279(2)	83.8(2)	1.3251
$GdCr_2Si_2C$	3.983(3)	5.263(3)	83.5(2)	1.3210
$TbCr_2Si_2C$	3.974(3)	5.244(3)	82.8(1)	1.3196
$DyCr_2Si_2C$	3.964(2)	5.214(4)	81.9(2)	1.3153
$HoCr_2Si_2C$	3.958(1)	5.213(3)	81.7(2)	1.3170
$ErCr_2Si_2C$	3.951(3)	5.191(5)	81.0(2)	1.3138
YCr_2Si_2C	3.969(2)	5.219(4)	82.2(1)	1.3149

IV. RESULTS AND DISCUSSION

A. Structural investigations of RCr_2Si_2C compounds

1. Powder experiments

Eleven RCr_2Si_2C compounds have been synthesized and checked with R=Y, La–Sm, Gd–Er. The indexation of the Guinier powder diagrams confirmed the space group $P4/mmm$ for all of these compounds. Lattice parameters, refined by a least square procedure, are gathered in Table II.

Diffraction patterns show unambiguously that R, Cr, and Si atoms occupy the 1(a), 2(e), and 2(h) crystallographic positions characteristic of the tetragonal $CeMg_2Si_2$-type structure. The latter can be obtained from the $ThCr_2Si_2$-type structure (space group $I4/mmm$) by a $[\frac{1}{2}, \frac{1}{2}, 0]$ translation of one X-R-X slab out of two (Fig. 1).

Thus, these two structural types differ only in the coordination of the transition metal, which is tetrahedral in $ThCr_2Si_2$ and rectangular in $CeMg_2Si_2$. Carbon atoms are located at the 1(b) position at the center of deformed "Cr_4R_2" octahedrons (or face-centered "Si_8Cr_4" square prisms). This result, in good agreement with previous studies,[8,9] was confirmed by single-crystal structure refinements and also by powder neutron-diffraction experiments (see below). Evolution of the lattice parameters and of the unit-cell volume with

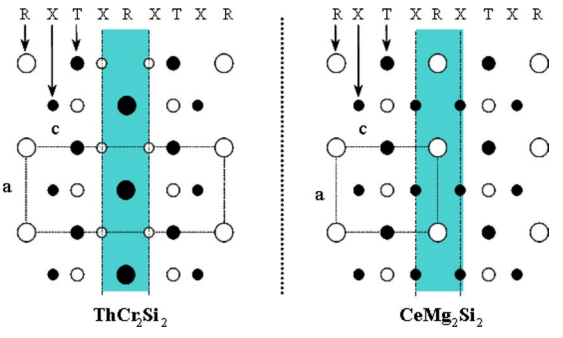

FIG. 1. (Color online) Projection of $ThCr_2Si_2$ and $CeMg_2Si_2$ structures along the [001] direction (black: $y=\frac{1}{2}$; white: $y=0$).

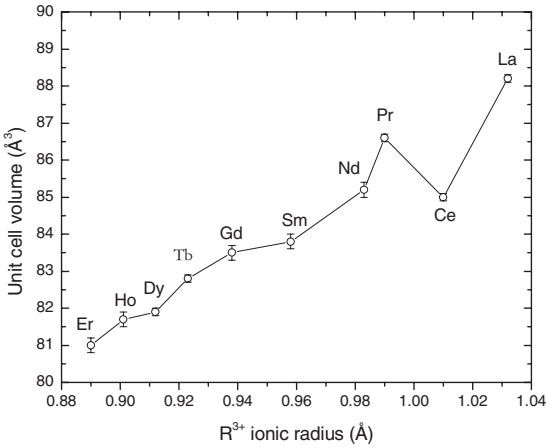

FIG. 2. Evolution of the unit-cell volume of RCr_2Si_2C compounds with respect to the R^{3+} ionic radius (R=La-Nd, Sm, Gd–Er).

respect to the trivalent R^{3+} ion radius (Fig. 2) suggests an intermediate-valence state for cerium in $CeCr_2Si_2C$.

Comparison between lattice parameters of quaternary RCr_2Si_2C compounds and corresponding ternary $ThCr_2Si_2$-type RCr_2Si_2 compounds (R=Sm, Gd–Er) shows that inserting carbon within the chromium (001) square planes results in an increase of the lattice parameter a (from 0.5% when R=Sm up to 1.6% when R=Er). On the contrary, the lattice parameter c in RCr_2Si_2C always remains lower than one half of the parameter c in RCr_2Si_2 (from 1.3% for R=Sm up to 2.1% for R=Er), thus suggesting covalent R-C bonds along the [001] direction.

2. Single-crystal experiments

In order to precisely determine crystallographic features and especially the evolution of interatomic distances, YCr_2Si_2C, $LaCr_2Si_2C$, and $SmCr_2Si_2C$ compounds have also been studied by means of single-crystal x-ray diffraction. The main crystallographic data obtained are reported in Table III.

Results unambiguously confirm all of the conclusions made from the powder study. Moreover, the carbon localization in 1(b) $(0, 0, \frac{1}{2})$ has been precisely confirmed using a Fourier difference procedure (FMAP 2 command in SHELX97 software[12]). However, the weak atomic scattering factor of carbon did not allow determining precisely, and unambiguously, its occupation rate. As detailed in Sec. IV C, powder neutron-diffraction data clearly showed that this occupation rate is equal to 1 in all the measured compounds.

Analysis of the main interatomic distances and of their relative dilatations Δ with respect to metallic radii (Table IV), reveals short Cr-C ($\Delta_{Cr\text{-}C}=-11$ to -12%) and R-C ($\Delta_{R\text{-}C}=-3$ to -4%) lengths, whereas Si-C distances are very large ($\Delta_{Si\text{-}C}>40\%$). These results suggest that the stability of quaternary RCr_2Si_2C compounds is mainly linked to the existence of covalent Cr-C and probably R-C bonds (see Sec. IV B).

It is important to note here that for R=Ho and Er, RCr_2Si_2C compounds were more difficult to obtain (and never obtained pure) than for the other R elements. More-

TABLE III. Atomic coordinates and thermal parameter of $LaCr_2Si_2C$, $SmCr_2Si_2C$, and YCr_2Si_2C.

Site	Atom	x	y	z	B_{eq} (Å^2)
YCr_2Si_2C (R=4.17%)					
1(a)	Y	0	0	0	0.56(4)
2(e)	Cr	0	$\frac{1}{2}$	$\frac{1}{2}$	0.62(4)
2(h)	Si	$\frac{1}{2}$	$\frac{1}{2}$	0.2268(4)	0.61(4)
1(b)	C	0	0	$\frac{1}{2}$	0.95(15)
$LaCr_2Si_2C$ (R=2.58%)					
1(a)	La	0	0	0	0.50(1)
2(e)	Cr	0	$\frac{1}{2}$	$\frac{1}{2}$	0.84(3)
2(h)	Si	$\frac{1}{2}$	$\frac{1}{2}$	0.2348(4)	0.58(3)
1(b)	C	0	0	$\frac{1}{2}$	1.26(16)
$SmCr_2Si_2C$ (R=2.86%)					
1(a)	Sm	0	0	0	0.69(6)
2(e)	Cr	0	$\frac{1}{2}$	$\frac{1}{2}$	0.69(6)
2(h)	Si	$\frac{1}{2}$	$\frac{1}{2}$	0.2279(7)	0.67(7)
1(b)	C	0	0	$\frac{1}{2}$	0.71(30)

over, no RCr_2Si_2C compound could ever be stabilized with R=Tm and Lu. This decreasing stability upon decreasing the size of R may be explained by simple steric considerations. Indeed, we observe that Cr-C distances decrease with the size of R. So there may be a critical R size leading to too short Cr-C bonds: for example, let us keep in mind that the Cr-C distance is 2.02 Å in the binary Cr_3C_2 compound, whereas Cr-C is as short as 1.98 Å in $ErCr_2Si_2C$.

B. Electronic structure of RCr_2Si_2C and RCr_2Si_2 (R=Y and La)

The detailed analysis of all site contributions to the density of states (Fig. 3) can give some insight into chemical bonding in RCr_2Si_2C compounds. The lowest bands ($-0.9 < E < 0.5$ Ry) are formed from s states of C and Si atoms but the main s-C peak has lower energy than the corresponding one detected on the Si site. This may indicate rather weak s-like bonding between Si and C atoms. Conversely, p orbitals of C and Si, lying in the energy range $-0.5 < E < -0.2$ Ry, strongly overlap. These p states also overlap the

TABLE IV. Interatomic distances (Å) and their relative evolutions in $LaCr_2Si_2C$, $SmCr_2Si_2C$ and YCr_2Si_2C compounds. Δ_{ij} (%)=$(100[d_{ij}-(r_i+r_j)])/(r_i+r_j)$ with d_{ij} the interatomic distance and r_i, r_j, metallic radius evaluated in Ref. 22.

	$LaCr_2Si_2C$		$SmCr_2Si_2C$		YCr_2Si_2C	
	d_{inter} (Å)	Δ (%)	d_{inter} (Å)	Δ (%)	d_{inter} (Å)	Δ (%)
4R-R	4.048(1)	+7.8	3.985(1)	+10.6	3.969(2)	+10.2
2R-C	2.691(1)	−3.7	2.639(1)	−2.9	2.609(2)	−4.0
8R-Si	3.129(1)	−2.1	3.064(2)	−1.8	3.046(2)	−2.4
8R-Cr	3.367(1)	+4.0	3.307(1)	+4.6	3.279(2)	+3.7
2Cr-C	2.024(1)	−11.1	1.992(1)	−12.5	1.985(1)	−12.8
4Cr-Cr	2.862(1)	+5.2	2.818(1)	+3.6	2.807(2)	+3.2
4Cr-Si	2.477(1)	−7.5	2.456(2)	−8.3	2.444(2)	−8.8
Si-Si	2.527(5)	−4.2	2.406(7)	−8.8	2.367(5)	−10.3
8Si-C	3.198(2)	+43	3.163(2)	+41	3.148(4)	+41

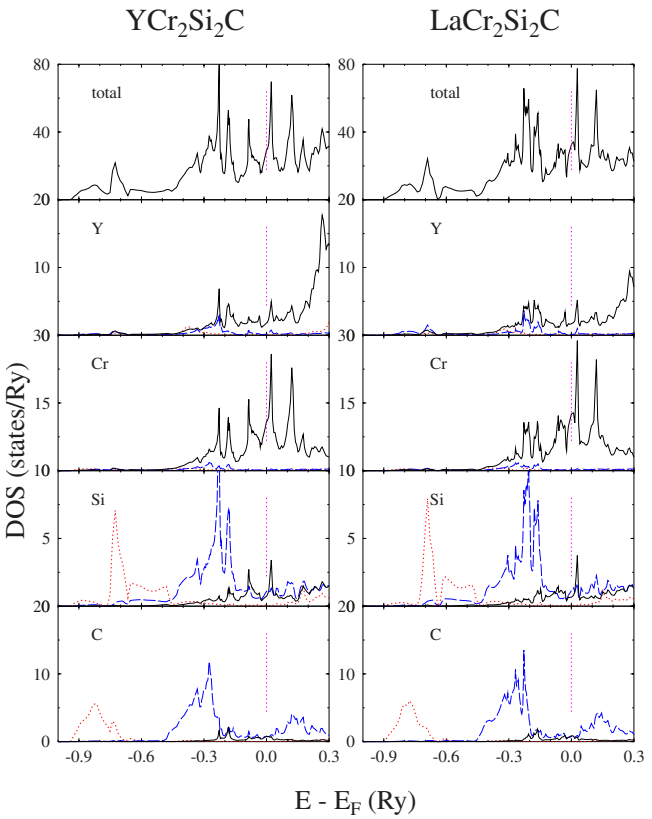

FIG. 3. (Color online) KKR total (top panel) and partial (for Y, Cr, Si, and C) density of states in RCr_2Si_2C (R=Y and La). In lower panels s, p, and d contributions to DOS are plotted with dotted, dashed, and solid lines, respectively.

TABLE V. Calculated electronic properties in RCr_2Si_2 ($ThCr_2Si_2$ type) and RCr_2Si_2C ("filled" $CeMg_2Si_2C$ type). Total DOS at E_F, $n_{tot}(E_F)$ (per f.u.), Cr d-DOS $n_{Cr\text{-}d}(E_F)$ Stoner product $I\, n_{Cr\text{-}d}(E_F)$ (I=0.032 Ry), as well as Cr magnetic moment in F and AF state are given.

Compound	$n_{tot}(E_F)$ (Ry^{-1})	$n_{Cr\text{-}d}(E_F)$ (Ry^{-1})	$I\, n_{Cr\text{-}d}(E_F)$	μ_{Cr} (F) (μ_B)	μ_{Cr} (AF) (μ_B)
YCr_2Si_2	133.6	54.8	1.75	0.96	2.01 (1.96)[a]
$LaCr_2Si_2$ [b]	142.3	54.1	1.73	1.1	2.32
YCr_2Si_2C	61.3	23.6	0.75	0	0
$LaCr_2Si_2C$	64.7	25.1	0.83	0	0

[a]Neutron-diffraction data (Ref. 1).
[b]Hypothetical but it can be stabilized with Fe, i.e., $LaCr_{2-x}Fe_xSi_2$ ($0.5<x<2$).

d states of the transition-metal sites (essentially on Cr). Note that the two DOS peaks appearing on Cr and Si, in the energy range of $-0.25<E<-0.15$ Ry, reflect rather important interactions between these atoms. It seems that the presence of C in the RCr_2Si_2C structure enhances the Cr-Si interactions with respect to those observed in the RCr_2Si_2 structure. This behavior is in line with the shorter distance between Cr planes in RCr_2Si_2C than the corresponding one in RCr_2Si_2.

The electronic states observed in the vicinity of the Fermi level are dominated by d states of Cr and R with some admixture of p states of C and Si. Notably, p states of C form a two-peak spectrum linked by a broad DOS minimum (near E_F), which can be regarded as a bonding and antibonding state separations (below and above the Fermi level, respectively). Such an electronic structure behavior suggests strong Cr-C interactions due to a short interatomic distance in the a-b plane, presumably responsible for a substantial decrease of the DOS near E_F in RCr_2Si_2C. Spin-polarized KKR calculations have also been made in YCr_2Si_2C and $LaCr_2Si_2C$ and all these computations converged into a nonmagnetic ground state (see also, Sec. IV E).

Comparing the DOS in YCr_2Si_2C and $LaCr_2Si_2C$ (Fig. 3), one can tentatively analyze the effect of interatomic distance dilatation on electronic structure, since the unit cell of the latter is expanded (see Tables I and IV).

At a first glance, we note that the valence bands in YCr_2Si_2C are broader than those calculated in $LaCr_2Si_2C$. This appears to be a consequence of stronger overlapping of the wave functions in the former. However, the cell volume increase (i.e., the Cr-C distance changes by about 1.4%) only slightly influences electronic states in the vicinity of the Fermi level, resulting in similar values of $n_{tot}(E_F)$ ~ 61 Ry^{-1} and ~ 64 Ry^{-1} in YCr_2Si_2C and $LaCr_2Si_2C$, respectively (see Table V).

In contrast to RCr_2Si_2C, the electronic structure of RCr_2Si_2 is much narrower and the DOS peaks are more pronounced, especially in the vicinity of the Fermi level. It also differs in the lower energy range ($-0.75<E<0.55$ Ry), where one can detect two energy gaps that are not present in C-containing samples (Fig. 4).

The first gap separates two s-like DOS peaks, attributed mainly to Si (also mixed with Y states), while the second one lies just below the p-d block consisting of d states of Cr and Y strongly hybridized with Si p states. The Fermi level was found in a large and narrow peak of nonspin-polarized DOS (Fig. 4), being formed essentially of d states from Cr. This DOS feature suggesting a local magnetic instability on Cr atoms was verified by the spin-polarized KKR calculations of RCr_2Si_2. These computations resulted in the Cr magnetic moment as large as 2.01 μ_B, when assuming experimentally detected AF structure [i.e., AF (001) planes coupled also AF, see Fig. 5], while only 0.95 μ_B in the hypothetical F state.

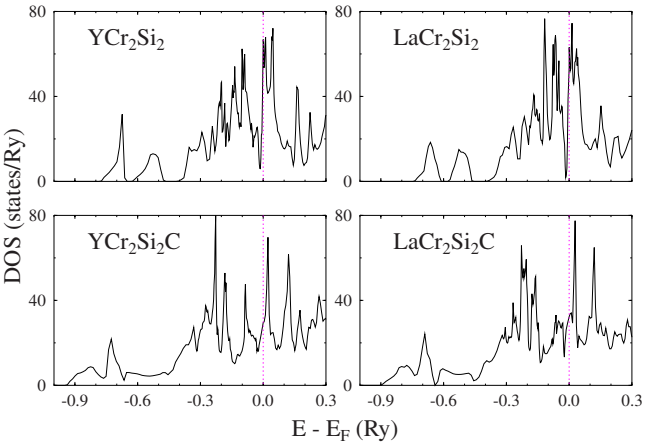

FIG. 4. (Color online) Comparison of KKR total DOS in RCr_2Si_2 ($ThCr_2Si_2$ type) and RCr_2Si_2C ($CeMg_2Si_2C$ type).

Such interesting behavior presumably comes from markedly different interatomic distance between the Cr atoms with parallel magnetic moments. The Cr-Cr distance is about 2.76 Å ($d_{Cr\text{-}Cr}=\sqrt{2}/2a$) when considering ferromagnetic ordering. This interatomic distance is almost 6 Å ($d_{Cr\text{-}Cr}=\frac{1}{2}\sqrt{2a^2+c^2}$, a, and c are lattice parameters) in the aforementioned AF structure. The theoretical magnetic moment on Cr ($\mu_{th}\sim 2.0$ μ_B) remains in excellent agreement with reported experimental neutron-diffraction data ($\mu_{exp}\sim 1.96$ μ_B).[1]

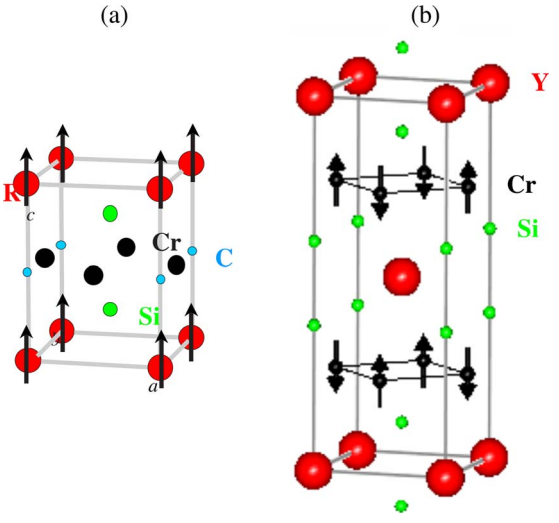

FIG. 5. (Color online) Magnetic structures at 2 K of (a) RCr_2Si_2C (R=Pr, Nd, Tb, Dy) and (b) YCr_2Si_2 compounds.

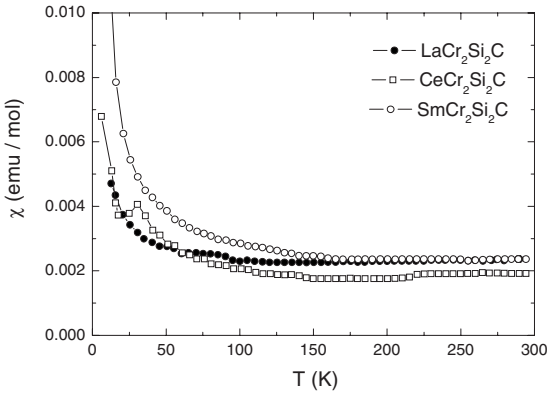

FIG. 6. Thermal variations of the magnetic susceptibility between 300 and 2 K for $LaCr_2Si_2C$, $CeCr_2Si_2C$, and $SmCr_2Si_2C$ (applied field=5 kOe).

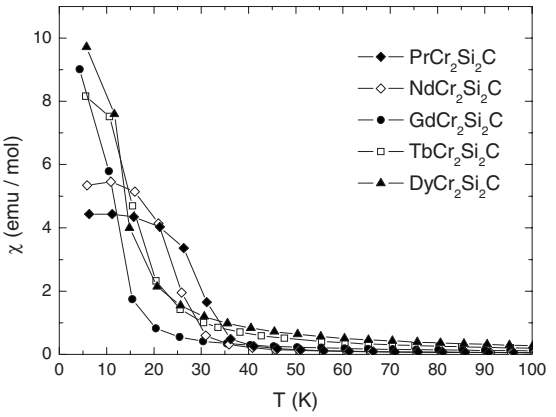

FIG. 7. Thermal variations of the magnetic susceptibility between 300 and 2 K for RCr_2Si_2C with R=Pr, Nd, Gd-Dy (applied field=5 kOe).

C. Magnetic study of RCr_2Si_2C compounds

1. Macroscopic measurements

Thermal variations of the magnetic susceptibility of zero-field cooled RCr_2Si_2C compounds (R=La-Nd, Sm, Gd–Dy) are displayed in Figs. 6 and 7. The main magnetic data are gathered in Table VI.

Unfortunately, too many magnetic impurities (mainly R-C and R-Si binary compounds) prevented us from studying the magnetic properties of Ho and Er compounds.

Magnetic susceptibilities of YCr_2Si_2C, $LaCr_2Si_2C$, and $CeCr_2Si_2C$ (Fig. 6) are very weak and temperature independent. Concerning $CeCr_2Si_2C$, the anomaly observed at 35(2) K should be attributed to the antiferromagnetic ordering of a CeC_2 impurity,[23] which was present in a low amount in our sample, as confirmed by the neutron-diffraction experiments. These three compounds thus exhibit a Pauli paramagnetic behavior in the whole temperature range. This result indicates that chromium does not carry any magnetic moment and confirms an intermediate-valence state of Ce in $CeCr_2Si_2C$, in good accordance with conclusions made from the lattice-parameter evolution.

Except for $SmCr_2Si_2C$, all other studied compounds (R=Pr, Nd, Gd–Dy) order ferromagnetically at low temperature ($T_C<35$ K) as shown in Fig. 7. In their paramagnetic state, the thermal dependence of the inverse susceptibility is well fitted by applying a modified Curie-Weiss law $\chi=\chi_0+C/(T-\theta_P)$, where C is the Curie constant and θ_P the paramagnetic Curie temperature; the temperature independent term χ_0 being close to 0.002 emu/mol. Effective magnetic-moment values are in good agreement with theoretical values for free R^{3+} ions. Paramagnetic Curie temperatures are slightly positive and very close to the ordering temperatures, indicating a ferromagnetic character of the main interactions (Table VI).

These measurements thus confirm the absence of a magnetic moment on the Cr sublattice in the RCr_2Si_2C compounds, contrary to what was previously observed with $ThCr_2Si_2$-type RCr_2Si_2 compounds (R=Y, Tb, Ho[1–3]).

Isothermal field dependences of the magnetization measured at $T=5$ K are displayed in Fig. 8.

Except for $GdCr_2Si_2C$ (probably because Gd^{3+} is an S-state ion), the shapes of these curves of first magnetization are characteristic of ferromagnetic compounds with non-negligible magnetocrystalline anisotropy: at low field ($H<3$ kOe), the Bloch walls do not move easily, and the magnetization increases quite slowly with H, reflecting the relative influence of magnetocrystalline anisotropy with respect to magnetic exchange. However, for all compounds, the coercive fields H_C remain quite low (Table VI).

TABLE VI. Main magnetic data of RCr_2Si_2C (R=La-Nd, Sm, Gd–Dy, Y) compounds (ncw is non-Curie-Weiss behavior).

Compound	T_C(±2 K)	θp(±5 K)	μ_{eff} (μ_B/mol)	M_{max} at 5 K (μ_B/mol)	H_C (±10 Oe)
YCr_2Si_2C	-	-	-	-	-
$LaCr_2Si_2C$	-	-	-	-	-
$CeCr_2Si_2C$	-	-	-	-	-
$PrCr_2Si_2C$	30	40	3.7	2.4	200
$NdCr_2Si_2C$	26	28	3.7	2.9	350
$SmCr_2Si_2C$	-	ncw	ncw	-	-
$GdCr_2Si_2C$	10	15	7.2	5.7	0
$TbCr_2Si_2C$	16	24	10.2	8.0	260
$DyCr_2Si_2C$	13	5	10.4	8.1	320

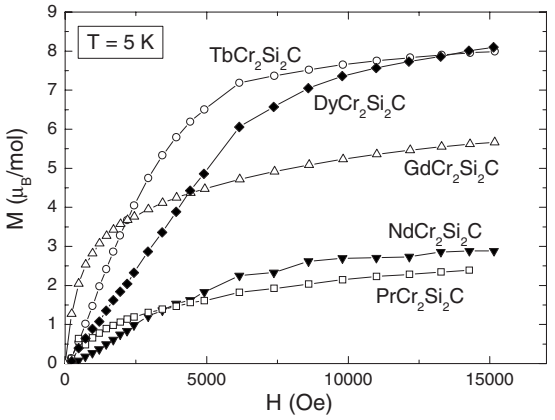

FIG. 8. Field dependence of magnetization in $R\mathrm{Cr_2Si_2C}$ (R=Pr, Nd, Gd–Dy) at T=5 K.

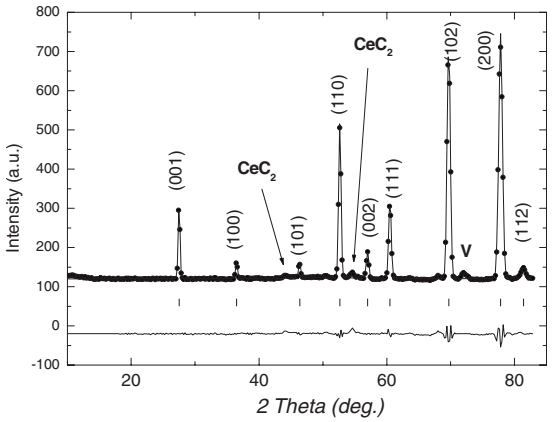

FIG. 9. Neutron powder-diffraction pattern of $\mathrm{CeCr_2Si_2C}$ obtained at 2 K. The dots represent the experimental data, and the continuous curve is the calculated diffractogram. The small vertical lines are the calculated *hkl* positions for nuclear cell and the bottom trace is the difference plot.

2. Neutron-diffraction experiments

A powder neutron-diffraction study was undertaken in order (i) to determine the carbon distribution in the crystallographic lattice, (ii) to confirm the absence of magnetic ordering of the chromium sublattice, and (iii) to determine the orientations, couplings, and amplitudes of R magnetic moments when the compounds are magnetically ordered.

Thermograms have been recorded in the temperature range 2–300 K, and long duration patterns have been recorded at 300 and 2 K. Neutron-diffraction patterns recorded at 300 and 2 K unambiguously confirm the $\mathrm{CeMg_2Si_2}$-type structure for all compounds, as deduced from the x-ray study.

D. $\mathrm{YCr_2Si_2C}$, $\mathrm{LaCr_2Si_2C}$ and $\mathrm{CeCr_2Si_2C}$

In good accordance with the absence of a magnetic moment on the chromium sublattice, as deduced from macroscopic magnetic measurements, no magnetic contribution to the intensities of the diffraction peaks could be detected over the whole temperature range. This study also confirms the absence of magnetic ordering of the cerium compound for $T \geq 2$ K (Fig. 9), which is consistent with an intermediate-valence state of this element.

The neutron-scattering length of carbon (b_{C}=6.648 fm) being of the same order of magnitude as the neutron-scattering lengths of chromium (b_{Cr}=3.635 fm), silicium (b_{Si}=4.151 fm), and lanthanides (b_Y=7.75 fm; b_{La}=8.24 fm; b_{Ce}=4.84 fm),[24] neutron diffraction allowed unambiguously locating carbon in 1(b) $(0, 0, \frac{1}{2})$ positions of the $\mathrm{CeMg_2Si_2}$-type structure, with refined values of occupation rates very close to 1 for each compound, thus justifying the $R\mathrm{Cr_2Si_2C}$ formula (Table VII).

E. $\mathrm{PrCr_2Si_2C}$, $\mathrm{NdCr_2Si_2C}$, $\mathrm{TbCr_2Si_2C}$, and $\mathrm{DyCr_2Si_2C}$

In the whole temperature range studied, neutron-diffraction patterns are quite similar for these four compounds. Only the Bragg-peak relative intensities differ from one compound to another due to different scattering lengths of the lanthanide element and to different ordered magnetic-moment amplitudes. For example, neutron thermograms recorded for $\mathrm{PrCr_2Si_2C}$ between 100 and 2 K are displayed in Fig. 10.

TABLE VII. Refined parameters and reliability factors for $R\mathrm{Cr_2Si_2C}$ (R=Y, La–Nd, Tb, Dy) compounds.

	T (K)	a (Å)	c (Å)	z_{Si}	f_{occ} (C)	μ_R (μB)	R_n (%)	R_m (%)	R_{wp} (%)	R_e (%)	f_{cor}
$\mathrm{YCr_2Si_2C}$	2	3.987(6)	5.238(1)	0.226(3)	0.98(2)	-	8.80	-	12.2	2.61	1.23(2)
$\mathrm{LaCr_2Si_2C}$	2	4.042(1)	5.372(2)	0.217(5)	0.99(1)	-	8.65	-	11.0	2.34	1.18(1)
$\mathrm{CeCr_2Si_2C}$	2	4.010(1)	5.273(1)	0.222(2)	0.98(2)	-	6.16	-	8.71	1.58	1.11(1)
$\mathrm{PrCr_2Si_2C}$	100	4.008(1)	5.325(2)	0.230(4)	0.98(2)	-	7.14	-	12.0	1.61	1.28(1)
	2	4.007(1)	5.323(1)	0.227(7)	0.98(2)	2.76(9)	6.65	7.51	12.0	0.87	1.29(1)
$\mathrm{NdCr_2Si_2C}$	100	4.004(2)	5.309(3)	0.216(7)	0.98(2)	-	3.80	-	10.0	3.59	1.14(2)
	2	4.002(1)	5.306(1)	0.211(8)	0.99(1)	3.47(14)	4.15	6.70	10.7	2.13	1.12(1)
$\mathrm{TbCr_2Si_2C}$	75	3.972(1)	5.229(2)	0.202(4)	0.98(2)	-	3.35	-	8.24	2.57	1.03(2)
	2	3.973(1)	5.230(1)	0.190(5)	0.98(2)	8.93(17)	5.49	3.63	6.88	1.84	1.01(1)
$\mathrm{DyCr_2Si_2C}$	145	3.963(3)	5.206(3)	0.228(9)	0.98(2)	-	5.41	-	10.6	3.37	1.07(2)
	2	3.962(1)	5.203(2)	0.223(9)	0.99(1)	9.14(30)	7.06	5.24	9.79	2.69	1.07(1)

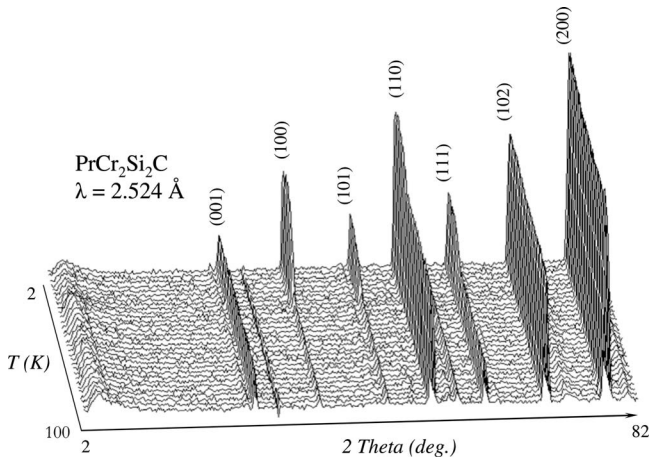

FIG. 10. Neutron thermogram of $PrCr_2Si_2C$ between 100 and 2 K.

Patterns recorded at high temperatures (greater than Curie temperatures) are very similar to those observed with the La and Ce compounds and thus lead to the same conclusions.

At 2 K, diffraction patterns are mainly characterized by the increase of some nuclear reflection intensities, indicating the ferromagnetic ordering of the compounds. The absence of any magnetic contribution to the intensities of (00*l*) reflections means that magnetic moments are orientated along the *c* axis. The magnetic structure of the RCr_2Si_2C compounds (R=Pr, Nd, Tb, Dy) is presented in Fig. 5. It can be described as a stacking of ferromagnetic (001) *R* planes along the *c* axis.

Refined values of the magnetic moments at 2 K ($\mu_{Pr}=2.76(9)\mu_B$; $\mu_{Nd}=3.47(14)\mu_B$; $\mu_{Tb}=8.97(17)\mu_B$; $\mu_{Dy}=9.14(30)\mu_B$) are very close to the theoretical values for the free R^{3+} ions (=g$J\mu_B$). Their temperature evolutions (Fig. 11) lead to deducing Curie temperatures equal to 33(1), 27(1), and 18(1) K for R=Pr, Nd, and Dy, respectively, in good accordance with the susceptibility results (Table VI).

In spite of the use of a special double-walled vanadium sample holder and of longer counting times, too much background, due to the huge neutron absorption cross section of Dy [994 barns at 0.0253 eV (Ref. 24)], and too incoherent scattering unfortunately prevented us from precisely deducing the Curie temperature of $DyCr_2Si_2C$ from this neutron experiment.

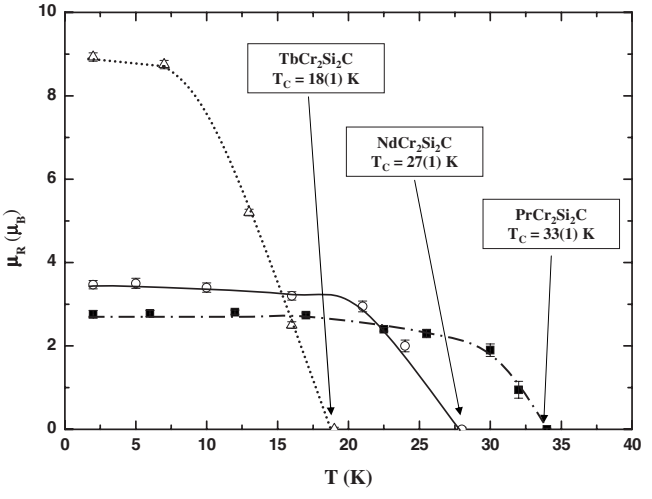

FIG. 11. Thermal evolution of magnetic moments (μ_R) deduced from neutron-diffraction experiments in RCr_2Si_2C compounds (R=Pr, Nd, Tb).

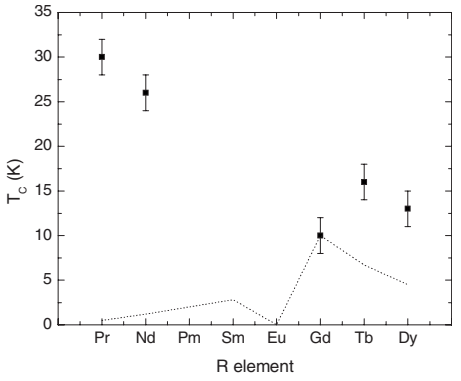

FIG. 12. Experimental Curie temperatures of RCr_2Si_2C compounds plotted with respect to the *R* element. The dotted line represents the corresponding ordering temperatures as calculated with the de Gennes rule (and normalized for R=Gd).

Finally, it is noteworthy that, at 2 K, despite a nonzero molecular field resulting from the ferromagnetic order of the *R* sublattice, no magnetic contribution from the Cr sublattice was ever detected.

F. Rare-earth magnetism in RCr_2Si_2C

RCr_2Si_2C compounds (R=Pr, Nd, Gd–Dy) are characterized by the ferromagnetic ordering of the lanthanide sublattice at very low temperatures ($T_C<35$ K). Figure 12 reports the measured Curie temperatures with respect to the *R* element.

From this plot, it is obvious that these temperatures do not follow a de Gennes[25] scaling. According to the de Gennes formulation, in the framework of the Ruderman-Kittel-Kasuya-Yosida (RKKY) theory of indirect exchange interaction, the magnetic ordering temperatures across a series of isostructural lanthanide-based compounds should be proportional to $(g_J-1)^2J(J+1)$, where g_J is the Landé factor and *J* is the total angular momentum of R^{3+}. In this way, the highest ordering temperature should be observed with the gadolinium compound, the total spin momentum *S* of Gd^{3+} being the largest among the lanthanides ($S=J=7/2$; $g_J=2$). But within the RCr_2Si_2C series, the Curie temperature of the Gd compound is lower than for other compounds. Thus, strictly speaking, the main interaction leading to the magnetic ordering of the *R* sublattice is not of the RKKY type.

Crystal-field effects may significantly affect ordering temperatures deduced from de Gennes rule:[26] crystal-field terms should then be added to the RKKY exchange Hamiltonian to obtain a correct formulation. The magnetic properties of RCr_2Si_2C compounds are likely influenced by crystal-field effects, the *R*-*R* interaction still being correctly described in the framework of the RKKY theory. Indeed, Gd^{3+} having a *S* ground state ($L=0$), it remains unaffected by the crystal field, to a first approximation, and the Curie temperature of the

corresponding compound thus remains proportional to the de Gennes factor. On the contrary, T_C of the other compounds may be enhanced under the effect of a crystal field.

It is interesting here to note that the $ThCr_2Si_2$-type RCr_2Si_2 compounds (R=Gd-Tm) exhibit lower ordering temperatures for the R sublattice than the corresponding RCr_2Si_2C compounds.[1] Indeed, e.g., in $GdCr_2Si_2$, the Gd sublattice orders antiferromagnetically at $T_N \sim 4.3$ K and the Tb sublattice orders at $T_N \sim 2.4$ K in $TbCr_2Si_2$. Shorter R-R distances across the Si-Cr_2-Si (or Si-[Cr_2, C]-Si) slabs may explain higher ordering temperatures in RCr_2Si_2C. For instance, at 300 K, Tb-Tb distances are equal to 5.675(1)Å in $TbCr_2Si_2$ (Ref. 1) and 5.244(3)Å in $TbCr_2Si_2C$. This shortening is due to the disappearance of the I Bravais mode when passing from $ThCr_2Si_2$ type to $CeMg_2Si_2$ type, probably associated with the creation of R-C bonds along [001]. However, R-R magnetic interactions remain quite low for both series of compounds.

Concerning the magnetocrystalline anisotropy, the easy magnetization direction, deduced at 2 K from neutron diffraction for R=Pr, Nd, Tb, and Dy, is always along the c axis. Lanthanide atoms occupy 1(a) (0, 0, 0) positions, with a tetragonal point symmetry $4/mmm$ (point group D_{4h}). In tetragonal symmetry, the easy magnetization direction of the R sublattice depends mainly on the sign of the second-order term of the crystal-field Hamiltonian B_2^0, which is given by $B_2^0 = \alpha_J \langle r^2 \rangle (1-\sigma_2) A_2^0$,[27] where α_J is the second-order Stevens coefficient for R^{3+},[28] σ_2 a screening parameter, and A_2^0 a parameter describing the electrostatic potential. An easy magnetization direction along [001] means a negative B_2^0.[27] Since α_J is negative for R=Pr, Nd, Tb, and Dy, we can deduce that A_2^0 is positive in RCr_2Si_2C compounds. Unfortunately, magnetic structures of Ho ($\alpha_J < 0$) and Er ($\alpha_J > 0$) compounds could not be determined during the present study due to the many impurity phases within the samples. But considering that A_2^0 does not vary significantly across the RCr_2Si_2C series, we expect the magnetic anisotropy of $HoCr_2Si_2C$ to be axial (magnetic moments along [001]) and of $ErCr_2Si_2C$ to be planar [magnetic moments within (001) planes].

G. Origin of Cr magnetic-moment quenching in RCr_2Si_2C

The question concerning the disappearance of magnetic ordering on the transition-metal sublattice in RCr_2Si_2C was addressed to analyze the Cr-DOS (particularly d states) in the vicinity of E_F. Table V gives the main electronic properties of RCr_2Si_2C compared to the corresponding values calculated in RCr_2Si_2 (R=Y and La). It is well established that the Stoner parameter on Cr calculated within the LDA approach provides predictions of a local magnetic moment onset on the site in transition-metal compounds. As mentioned in Sec. IV B, the carbon insertion in the Cr square planes leads to strong Cr-C interactions and results in substantial lowering of the DOS near E_F (Figs. 3 and 4). Indeed, the d contribution on Cr $n_{\text{Cr-}d}(E_F)$ was found well below the Stoner limit [$I\ n_{\text{Cr}}(E_F) \sim 0.75$], with I=0.032 Ry for d states from the KKR method. Since the insertion of C brings about the crystal structure transition, it was of interest to calculate the electronic structure and the Stoner product in the "filled"

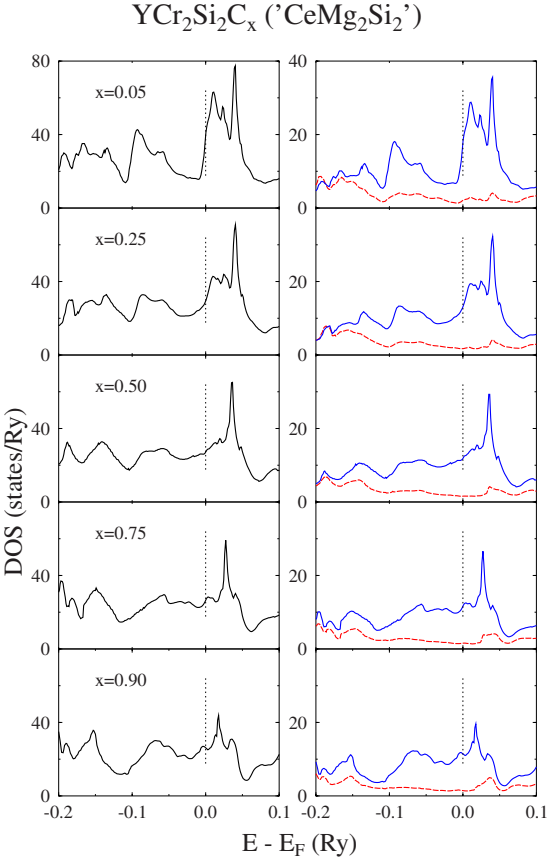

FIG. 13. (Color online) Evolution of the nonspin-polarized KKR-CPA DOS in $YCr_2Si_2C_x$ ("filled" $CeMg_2Si_2$ type) close to the Fermi level. The rapid DOS decrease at E_F is observed, when C content increases and a local minimum is developed at high x. The blue solid and red dashed lines represent d states of chromium and yttrium, respectively.

$ThCr_2Si_2$ type RCr_2Si_2C. Quite similar results were obtained since $n_{\text{Cr-}d}(E_F) \sim 27$ Ry^{-1} was also found below the border of magnetic instability [$I\ n_{\text{Cr}}(E_F) \sim 0.85$]. However, the overall DOS shape as well as electronic structure details near E_F are rather different in the two structural variants (see Figs. 13 and 14).

The DOS characteristics in both structure types allow concluding that the electronic interactions between d-Cr and p-C atoms (also with p-Si), manifested by the appearance of bonding and antibonding DOS peaks on C and Si DOS, are predominantly responsible for a strong decrease of the DOS close to E_F, with respect to DOS characteristics detected in RCr_2Si_2. As shown in Table V, the values of $n_{\text{Cr}}(E_F)$ in RCr_2Si_2C are markedly lower than the corresponding ones computed in RCr_2Si_2 compounds (see also Fig. 4) and the Stoner criterion is fulfilled exclusively in the latter. This electronic structure behavior presumably drives the magnetism quenching in RCr_2Si_2C compounds and the arrangement of the R and Si plane stacking along the c axis, giving rise to tetragonal simple or body-centered crystal structures, appears to be less important as regards to the disappearance of a magnetic moment on the Cr atoms.

To better illustrate the effect of the vanishing of local magnetic moments in the AF ordering upon C filling in

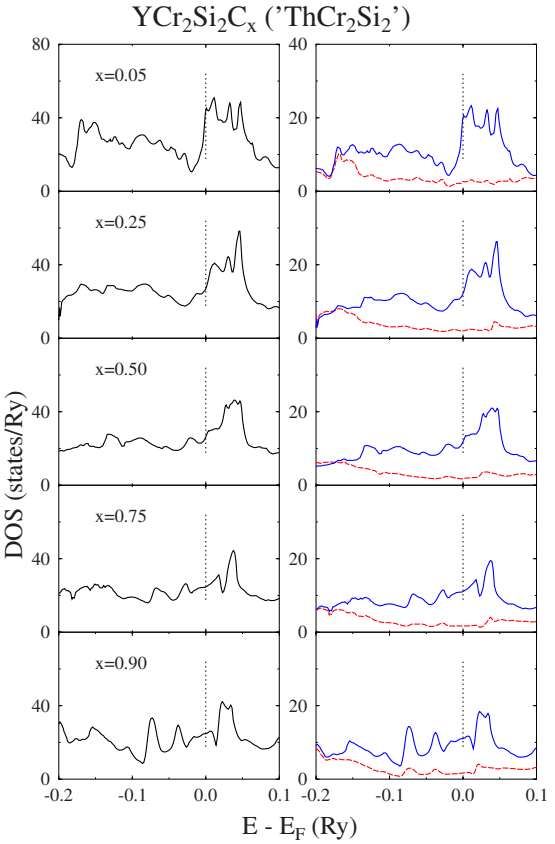

FIG. 14. (Color online) Evolution of the nonspin-polarized KKR-CPA DOS in $YCr_2Si_2C_x$ ("filled" $ThCr_2Si_2$ type) close to the Fermi level. The rapid DOS decrease at E_F is observed when C content increases but a broad maximum develops at high x. The blue solid and red dashed lines represent d states of chromium and yttrium, respectively.

RCr_2Si_2, electronic structures of "filled" $ThCr_2Si_2$ type as well as of "filled" $CeMg_2Si_2$-type $YCr_2Si_2C_x$ were calculated using the KKR-CPA method (accounting for a chemical disorder). Noteworthy, within these simulations, the crystal structure of YCr_2Si_2 ($ThCr_2Si_2$ type) or YCr_2Si_2C (filled $CeMg_2Si_2$ type) was real, whereas those of YCr_2Si_2C (filled $ThCr_2Si_2$ type) and YCr_2Si_2 ($CeMg_2Si_2$ type) were hypothetical. In both cases, carbon atoms randomly occupied the center of the Cr square in the unit cell and the C concentration was varied in a continuous way ($0.05<x<0.95$). Figures 13 and 14 present the evolution of the nonspin-polarized electronic structure from "magnetic" YCr_2Si_2 (high DOS near E_F) to "nonmagnetic" YCr_2Si_2C (low DOS near E_F) in both structural variants. We observe that even at small C concentrations in $YCr_2Si_2C_x$ ($x\sim0.25$), the Cr-C and Si-C interactions are so strong that the DOS at E_F dramatically decreases and the Stoner condition for the magnetism onset $[I\ n(E_F)>1]$ is no more fulfilled. At low C content, the DOS modifications are quite similar in both structural variants, except for the fact that the DOS near E_F decreases more rapidly with x in the "$CeMg_2Si_2$-type" model. Subtle differences in electronic spectra appear in C-rich samples ($x\sim0.9$) since one observes developing of a local DOS minimum in the vicinity of the Fermi level in the "$CeMg_2Si_2$-type" model (Fig. 13), whereas a broad DOS maximum in the "$ThCr_2Si_2$-type" one (Fig. 14). Finally, YCr_2Si_2C exhibits the value of $n(E_F)\sim61$ Ry^{-1} in the real structure, which is much lower than $n(E_F)\sim76$ Ry^{-1} computed in the hypothetical structure. All these electronic structure calculations tentatively support the experimentally observed change of the crystal structure when comparing YCr_2Si_2 and YCr_2Si_2C. The aforementioned analysis based on the Stoner criterion and nonspin-polarized DOS was well supported by the spin-polarized KKR-CPA computations in the "filled" $ThCr_2Si_2$-type $YCr_2Si_2C_x$ (assuming AF state). They showed that the magnetic moment on Cr rapidly decreased with C content, from 1.75 μ_B ($x=0.05$) to ~1 μ_B ($x=0.25$) and it vanishes for $x\sim0.5$.

The comparison of the KKR total energy calculated in YCr_2Si_2C and $LaCr_2Si_2C$ in both structural types also supports the crystal structure transformation upon C insertion, since conserving the same unit-cell volume in both structure types, the "filled" $CeMg_2Si_2$ type was favored. However, a more reliable explanation of this structural transition could be made if relaxing atom positions and a volume cell in total-energy computations of disordered $YCr_2Si_2C_x$ were obtained.

V. CONCLUSIONS

The experimental and theoretical results obtained during the present study on the RCr_2Si_2C compounds allow a better understanding of the carbon influence both on structural and magnetic properties. The main conclusions are summarized below.

(i) Carbon induces a structural transition from the $ThCr_2Si_2$ type (space group $I4/mmm$) to the "filled" $CeMg_2Si_2$ type (space group $P4/mmm$). This transition is tentatively supported by the total-energy calculation favoring the experimentally observed crystal structure upon comparing both carbon "filled" $ThCr_2Si_2$ and $CeMg_2Si_2$-type structures.

(i) Carbon insertion drastically affects the magnetic behavior since chromium does not have any magnetic moment in RCr_2Si_2C compounds, in contrast to RCr_2Si_2 compounds. This is well explained from the KKR-CPA computations performed for the $YCr_2Si_2C_x$ system ($0.05\leq x\leq0.95$), which evidenced a strong lowering of the DOS near E_F when the carbon content x increased (whatever the structure type). Consequently, the d-Cr states are rapidly found below the Stoner limit when x increases. This behavior was confirmed by the spin-polarized KKR-CPA calculations in antiferromagnetic $YCr_2Si_2C_x$ resulted in the Cr magnetic moment vanishing for $x>0.5$. RCr_2Si_2C ($R=Y$ and La) exhibit a nonmagnetic ground state, which is consistent with their Pauli paramagnetic properties and neutron powder measurements. On the other side of the system, YCr_2Si_2, as deduced from the neutron-diffraction study, is a strong antiferromagnet with the Cr moment as large as 1.96 μ_B, which is in fair agreement with the KKR calculated value of 2.01 μ_B.

(ii) Neutron powder-diffraction measurements performed on the RCr_2Si_2C compounds ($R=$Pr, Nd, Tb, Dy) evidenced a ferromagnetic ordering of the lanthanide sublattice at low temperature, the highest T_C being close to 30 K for $R=$Pr.

Thus, carbon also induces a change in the sign of the *R*-*R* couplings, the latter being antiferromagnetic in RCr_2Si_2 and becoming ferromagnetic in RCr_2Si_2C.

(iii) The $CeCr_2Si_2C$ compound is found to exhibit a Pauli paramagnetic behavior (and thus no magnetic ordering down to 2 K) linked to an intermediate-valence state of cerium. This compound is thus of special interest from the more fundamental point of view. Complementary experiments should be considered on this compound, such as x-ray absorption spectroscopy, and especially electrical resistivity measurements (to show, e.g., a potential Kondo behavior) at ambient as well as at high pressures.

ACKNOWLEDGMENTS

The authors thank the CRG-CNRS and the Institut Laue Langevin for the neutron beam time. One of us (J.T.) would like to express his thanks to LCSM UHP Nancy I (France). This work was partly supported by the KBN Grant No. N202 2104 33.

*Present address. CEA, IRAMIS, Laboratoire Léon Brillouin, 91191 Gif-sur-Yvette Cedex, France.

[1] I. Ijjaali, Ph.D. thesis, Université Henri Poincaré Nancy, 1999.
[2] O. Moze, M. Hofmann, J. M. Cadogan, and K. H. J. Buschow, J. Alloys Compd. **308**, 60 (2000).
[3] O. Moze, M. Hofmann, J. M. Cadogan, and K. H. J. Buschow, Eur. Phys. J. B **36**, 511 (2003).
[4] J. Tobola, B. Malaman, and G. Venturini, Acta Phys. Pol. A **97**, 761 (2000).
[5] B. Malaman, G. Venturini, A. Blaise, J. P. Sanchez, and G. Amoretti, Phys. Rev. B **47**, 8681 (1993), and references therein.
[6] G. Venturini, E. Ressouche, and B. Malaman, J. Alloys Compd. **241**, 135 (1996).
[7] B. Malaman, G. Venturini, G. Le Caër, and J. Tobola, Proceedings of the 15th International Conf. on Solid Compounds of Transition Elements, Krakow (2006).
[8] C. Tang, S. Fan, and M. Zhu, J. Alloys Compd. **299**, 1 (2000).
[9] M. W. Pohlkamp and W. Jeitschko, Z. Naturforsch., B: Chem. Sci. **56**, 1143 (2001).
[10] V. Klosek, Ph.D. thesis, Université Henri Poincaré- Nancy, 2002.
[11] Z. Otwinowski and W. Minor, *Macromolecular Crystallography Part A: Methods in Enzymology*, edited by C. W. Carter Jr. and R. M. Sweet (Academic, New York, 1997), Vol. L76, p. 307.
[12] G. M. Sheldrick, *SHELXL97, Program for the Refinement of Crystal Structures* (University of Gottingen, Germany, 1997).
[13] R. H. Blessing, Crystallogr. Rev. **1**, 3 (1987).
[14] www.ill.eu/d1b/home/
[15] J. Rodriguez-Carvajal, Physica B (Amsterdam) **192**, 55 (1993).
[16] *Applications of Multiple Scattering Theory to Materials Science*, MRS Symposia Proceedings No. 25, edited by W. H. Butler, P. H. Dederichs, A. Gonis, and R. Weaver (Materials Research Society, Pittsburgh, 1992), Chap. III.
[17] S. Bei der Kellen, Yoosik Oh, E. Badralexe, and A. J. Freeman, Phys. Rev. B **51**, 9560 (1995).
[18] T. Stopa, S. Kaprzyk, and J. Tobola, J. Phys.: Condens. Matter **16**, 4921 (2004).
[19] J. P. Perdew and Y. Wang, Phys. Rev. B **45**, 13244 (1992).
[20] S. Kaprzyk and A. Bansil, Phys. Rev. B **42**, 7358 (1990).
[21] A. Bansil, S. Kaprzyk, P. E. Mijnarends, and J. Tobola, Phys. Rev. B **60**, 13396 (1999).
[22] Teatum *et al.*, in *The Crystal Chemistry and Physics of Metal and Alloys*, edited by W. B. Pearson (Wiley, New York, 1972).
[23] M. Atoji, J. Chem. Phys. **46**, 1891 (1967).
[24] V. F. Sears, Neutron News **3**, 26 (1992).
[25] P. G. de Gennes, J. Phys. Radium **23**, 510 (1962).
[26] D. R. Noakes and G. K. Shenoy, Phys. Lett. **91A**, 35 (1982).
[27] J. E. Greedan and C. N. Rao, J. Solid State Chem. **6**, 387 (1973).
[28] K. W. H. Stevens, Proc. Phys. Soc., London, Sect. A **65**, 209 (1952).